A novel analytical model for the transit time distributions in urban groundwater systems

Miao Jing[1,2], Chunhui Lu[1,2]*, Falk Heße[3], Rohini Kumar[3]

[1] State Key Laboratory of Hydrology-Water Resources and Hydraulic Engineering, Hohai University, 210098 Nanjing, China

[2] Yangtze Institute for Conservation and Development, Hohai University, 210098 Nanjing, China

[3] Department of Computational Hydrosystems, Helmholtz Centre for Environmental Research – UFZ, Permoserstr. 15, 04318 Leipzig, Germany

*corresponding author: clu@hhu.edu.cn

Revised manuscript submitted to *Journal of Hydrology* on Aug 17, 2021

Highlights:

1. An analytical model for urban groundwater TTDs is developed.

2. The imperviousness significantly affects groundwater TTDs.

3. Depth of the underground structure strongly controls groundwater TTDs.

Abstract

With the ongoing rapid urbanization across the globe, its interference with groundwater resources is critical to freshwater sustainability. The groundwater transit time distribution (TTD) lumps the flow and transport processes of a regional groundwater system and therefore characterizes the aquifer's resilience to nonpoint-source contamination. The influence of large-scale urban areas on the regional groundwater TTD is not clear. This study proposed a novel analytical model for groundwater TTDs accounting for the effects of impervious urban structures. After the verification against results from particle tracking, we apply this analytical expression to investigate how the position and spatial extent of the urban area change the TTDs from the pre-urban ones. The sensitivity analysis suggests that urban areas tend to increase both the mean and the variance of groundwater transit times. For aquifers intersected by a local urban area, mean transit time (MTT) is dominated by the horizontal extent of the urban area, whereas for aquifers intersected by a regional urban area, MTT is strongly controlled by the vertical extent of the urban area in addition to its horizontal size. Modeling results highlight the importance of the spatial relationship between the urban area and the aquifer in determining the urban groundwater TTDs. Being computationally efficient, the proposed analytical model can aid decision-making in urban freshwater resources management and urban planning.

1 Introduction

Rapid urbanization threatens the safety and sustainability of freshwater resources, especially in developing countries. In 2014, around 3.9 billion people lived in cities, and this number is expected to rise to two-thirds of the global population in 2050 (Connor, 2015). Urbanization and the improvement of living standards lead to increasing demand for water in cities (Connor, 2015). Besides, rapid urbanization modifies the water cycle in several ways. Cities extract substantial amounts of water from streams and groundwater and challenge the sustainability of regional water resources (Larsen et al., 2016; Ostad-Ali-Askari & Shayannejad, 2021). Besides, urbanization also extends the area of impervious surface and prevents groundwater recharge, therefore causing higher flood risks (Golian et al., 2020; Vázquez-Suñé et al., 2005). Finally, urbanization may threaten the downstream surface water body by discharging pollutants from cities.

In this context, urban aquifers play a critical part in sustaining the urban water supply and must be integrated into the strategies of water resources management. On one hand, the expansion of impervious areas may reduce groundwater recharge and further reduce baseflows, although the actual baseflow in urban watersheds can be increased by anthropogenic influences (Bonneau et al., 2018; Lerner, 2002; Ostad-Ali-Askari et al., 2019; Vázquez-Suñé et al., 2010). On the other hand, modern construction technologies tend to extend not only the area but also the depth of the urban impact region, which typically cuts the aquifer and alters the local and regional groundwater flow field (Attard et al., 2017; Font-Capo et al., 2015; Ostad-Ali-Askari et al., 2020; Pujades et al., 2012).

Most of the previous works have investigated the influence of urbanization on groundwater quantity and flux-related aspects (Attard, Winiarski, et al., 2016). Underground structures intersecting the confined aquifer may exert a barrier effect on groundwater heads, which can be expressed as the increase in head difference across the underground structure after the construction (Pujades et al., 2012, 2016). This barrier effect may cause many environmental problems such as ground settlements (Xu et al., 2019) and contaminants mobilization (Font-Capo et al., 2015; Jurado et al., 2012). Many other studies have focused on the modification in water budget partitioning and baseflow generation (Bhaskar et al., 2016; Bonneau et al., 2017; Hamel & Fletcher, 2014; Janke et al., 2014; Schwartz & Smith, 2014). Despite these works, few have focused on the modification in water transit times in urban aquifers.

For a local/regional groundwater system, transit/travel time is defined as the time spent by a water parcel from its entrance as recharge till its discharge into the surface water body (i.e., streams, lakes, or seas). Transit/travel time distribution (TTD) is the distribution of transit times, and it provides a lumped description of the transport and mixing processes in a regional aquifer system. Groundwater TTDs have important implications for the interpretation of tracer data (Benettin et al., 2015; Kuppel et al., 2020; Małoszewski & Zuber, 1982; Stewart et al., 2010; Zuber, 1986), biogeochemical processes (Van Der Velde et al., 2010), groundwater vulnerability to nonpoint-source contamination (Basu et al., 2012; Jing et al., 2019; Kumar et al., 2020; Ostad-Ali-Askar et al., 2018), and groundwater response to external changes including climate change (Engdahl & Maxwell, 2015; Havril et al., 2018; Jing et al., 2020). The mean transit time (MTT) of groundwater in an aquifer system ranges typically from years to decades, which is highly relevant to the lag in streamwater response to nonpoint-source pollutants. Employing simple lumped parameter models (Ginn et al., 2009; Małloszewski & Zuber, 1992; McCallum et al., 2015), transient travel time models (Asadollahi et al., 2020; Benettin et al., 2017; Heße et al., 2017), or particle-tracking models (Danesh-Yazdi et al., 2018; Eberts et al., 2012; Jing et al., 2021; Remondi et al., 2019), many studies have assessed the responses of streamwater to agricultural nonpoint-source contamination through deducing TTDs.

The climate forcing, topography, geometry, and hydraulic properties of aquifers cause TTDs to present unique shapes that reflect the transport and mixing processes within the aquifer (Abrams & Haitjema, 2018; Jing et al., 2019; Leray et al., 2016; Talebmorad et al., 2021). Many analytical solutions have been reported for catchments or aquifers, among which the exponential model is one of the most popular models (Eriksson, 1958; Haitjema, 1995; Luo & Cirpka, 2008; Małoszewski & Zuber, 1982). Analytical models bridge the gap between observations and the systems' intrinsic properties, which helps to understand why the real-world aquifer systems deviate from the reference ones (Leray et al., 2016). Unfortunately, most analytical models about groundwater TTDs assume natural conditions, with few considering the disturbance of urbanization on their shape and breadth.

Despite some previous studies that have employed the tracer data to infer the transit times in urban catchments and aquifers, these tracer-based studies often apply presumed lumped parameter models that typically fit the natural aquifers rather than urban aquifers (Hrachowitz & Clark, 2017; Kuhlemann et al., 2020; McCance et al., 2018; Soulsby et al., 2015). Moreover, presuming simple travel-time models without considering the impact of impervious urban zones may bias the interpretation of tracer data and cause unrealistic results (Jing et al., 2019; McCallum et al., 2015). With the development of modern construction techniques such as the cut and cover method, the urban structure often intersects with the water table and obstructs the natural groundwater flow, which could also strongly regulate the transport process and the transit times (Attard, Rossier, et al., 2016; Font-Capo et al., 2015). Consequently, it is useful to derive explicit expressions for groundwater TTDs in urban aquifers accounting for the influence of such impervious urban structures.

In this paper, we aim to quantify the influence of impervious urban construction on the shape and breadth of groundwater TTDs by deriving novel analytical solutions. In doing so, we expect to answer the following scientific questions: (1) How does the impervious urban area affect the regional-scale groundwater TTDs? (2) What is the most important factor that causes the deviation of groundwater transit times from the pre-urban ones? (3) How can we take adaptive strategies to reduce environmental risks caused by the modification in groundwater transit times? To answer these questions, we start by deriving novel analytical solutions for an idealized aquifer intersected by an urban sealing area. We then verify the analytical solutions by comparing them with numerical simulations and conduct a comprehensive parametric study under different scenarios considering a range of parameters of analytical expressions. Finally, we discuss the results and their implications for urban water resources management and urban planning.

2 Model and Methods

2.1 Problem description

This study focuses on the saturated groundwater system in an unconfined aquifer intersected by an impervious urban area. Compared to deep confined aquifers, shallow unconfined aquifers are more vulnerable to urban constructions and typically interact more actively with surface water, which is of great concern from an environmental perspective. The geometry and boundary conditions (BCs) of real-world watersheds are typically very complex, which hinders the derivation of analytical solutions (Fig. 1a). For the sake of simplification, we consider an idealized rectangular aquifer bounded by an upgradient natural groundwater divide and a downgradient water body (Fig. 1b and c). The upgradient and downgradient boundaries are assigned with a no-flux BC and a fixed-head BC, respectively. This aquifer is embedded in an aquitard and therefore, the lateral boundaries are also impervious. The discharge zone is at the downstream limit, which is normally a body of impounded surface water such as a river, a lake, or a sea. The groundwater flow is at steady state, meaning that the outflow equals the total amount of recharge. We only consider the groundwater flow in the saturated zone, which is assumed to be purely advective.

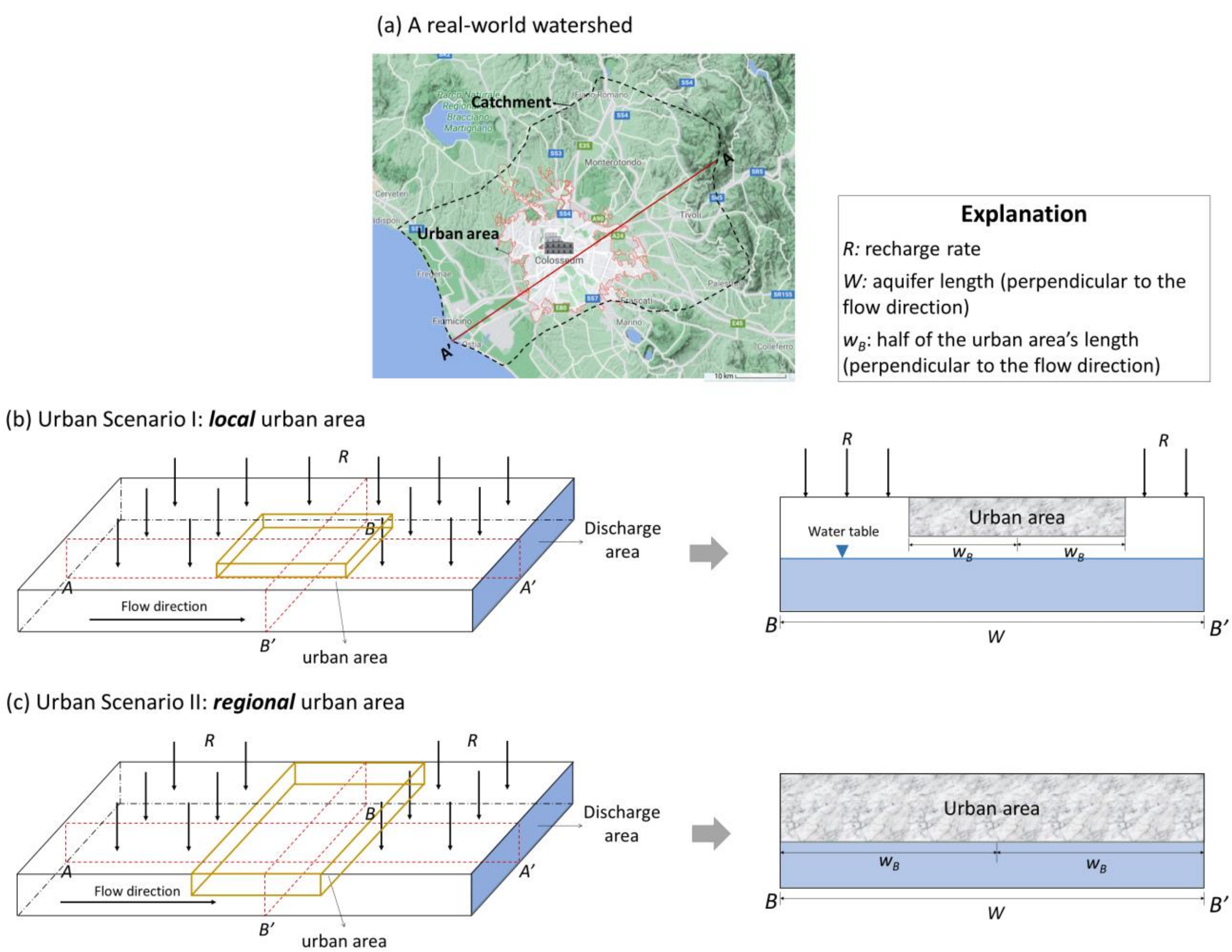

Fig. 1. Conceptualization of a regional aquifer system intersected by an urban area. A real-world watershed (a) is conceptualized into two scenarios: aquifers intersected by a local urban area (b) and aquifers intersected by a regional urban area (c).

The groundwater flow is horizontal based on the Dupuit-Forchheimer assumption (Dupuit, 1863; Forchheimer, 1886). This can be justified since the thickness of the saturated aquifer is typically small relative to its horizontal length, and the vertical component of flow velocity is neglectable relative to the horizontal one. Therefore, the groundwater head and velocity do not change with depth. The upper surface of the unconfined aquifer receives a uniform diffuse recharge, R [LT^{-1}], except for the impervious urban area (Fig. 1b and Fig. 1c). An impervious urban area seals the ground and prevents infiltration, and therefore no recharge occurs in this area. This is an idealized case because, in reality, leakages from water mains or sewage systems often significantly recharge groundwater (Vázquez-Suñé et al., 2005). Horizontally, the urban area is rectangular with a length of $2w_A$ at the flow direction (A-A' in Fig. 1) and a length of $2w_B$ perpendicular to the flow direction (B-B' in Fig. 1). The bottom of the urban structure can be either higher or lower than the water table under natural conditions.

Depending on the spatial extent of urban areas interacting with groundwater flows, we categorize them into local urban areas and regional urban areas. In cases that the urban structure is above the natural water table, it is defined as a local urban area (Fig. 1b). The local urban area does not confine the aquifer section since the phreatic surface exists alongside the local urban area. This urban scenario is named Urban Scenario I. If the urban structure is deep enough to intersect with the water table and large enough to fully penetrate the horizontal boundaries of the aquifer, it is defined as a regional urban area (Fig. 1c), and this scenario is named Urban Scenario II. In this scenario, the urban structure partially confines the aquifer (Fig. 1c). Because this study aims to unveil the alteration of urban construction on regional groundwater TTDs, we first introduce the analytical solution for the pre-urban scenario and then derive the analytical solutions for the urban scenarios.

2.2 Solutions in the pre-urban scenario

We consider a 2-D cross-sectional model for the derivation of analytical solutions in the pre-urban scenario (Fig. 2a). The water table (*h*) against distance (*x*) at this cross-section can be expressed using the Dupuit-Forchheimer ellipse (Dupuit, 1863):

$$h(x) = \sqrt{\frac{R}{K}(L^2 - x^2) + h_L^2} \tag{1}$$

where L is the length of the aquifer [L], R is the recharge rate [LT^{-1}], K is the saturated hydraulic conductivity [LT^{-1}], and h_L is the fixed head at the downstream boundary.

Given that the groundwater mounding is small to moderate, the groundwater TTDs can be modeled as an exponential function (Haitjema, 1995; Leray et al., 2016; Raats, 1977):

$$\rho(a) = \frac{1}{\tau_p}\exp\left(-\frac{1}{\tau_p}\right) \tag{2}$$

where τ_p is the MTT, which is controlled by the system's properties:

$$\tau_p = \frac{\theta \bar{H}}{R} \tag{3}$$

where θ is the effective porosity of aquifer [-], $\overline{H}$ is the mean saturated thickness [L], and R is the recharge rate [LT^{-1}]. The mean saturated thickness for the unconfined aquifer, $\overline{H}$, is expressed by Eq. (36) in Appendix A.

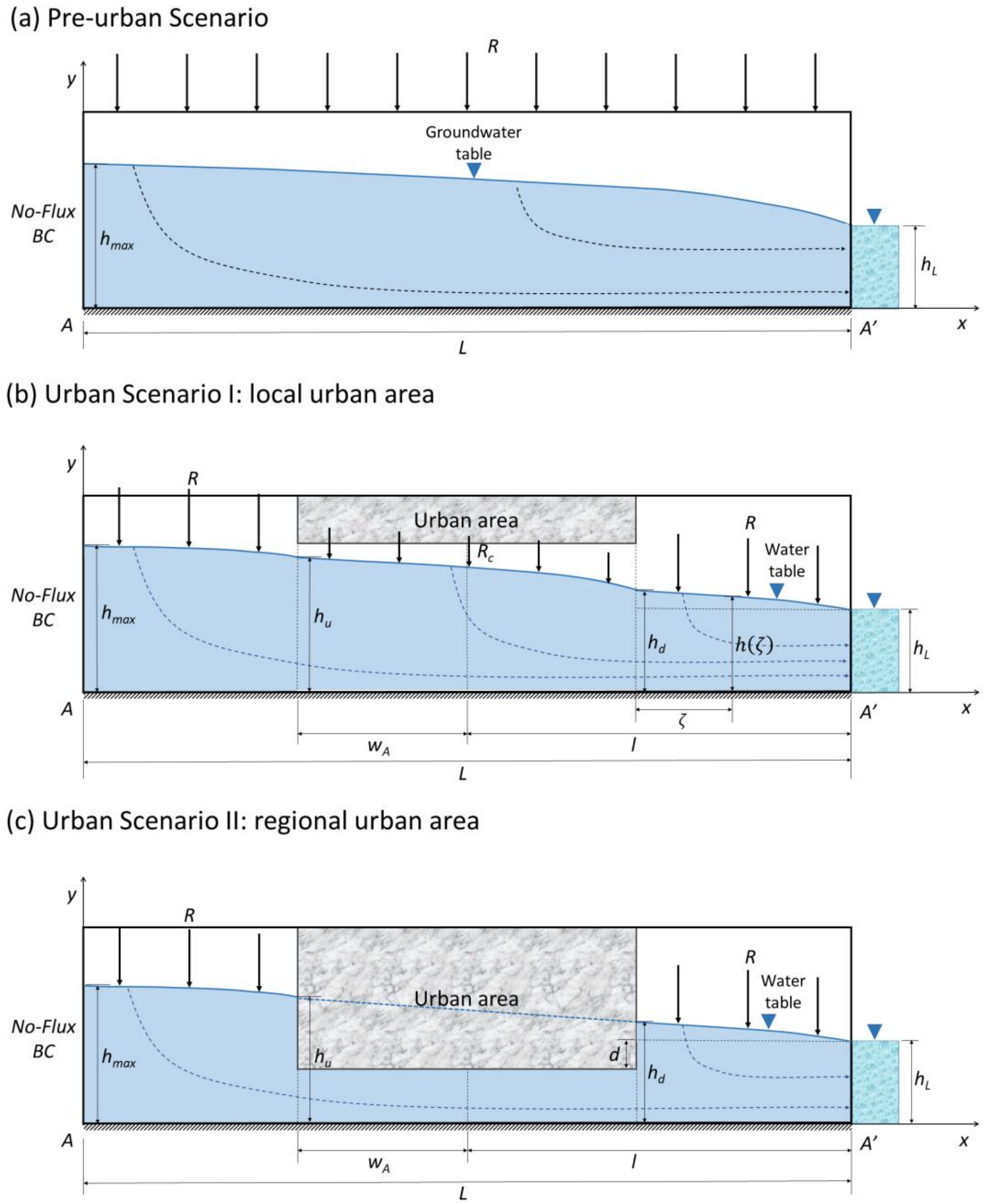

Fig. 2. Cross-sectional models (A-A' in Fig. 1) of the regional aquifer system in pre-urban and urban scenarios.

2.3 Solutions in the urban scenarios

In the urban scenario, the urban area divides the A-A' cross-section of the unconfined aquifer into three compartments: the upgradient zone, the urban area, and the downgradient zone (Fig. 2). The upgradient and downgradient zones have a recharge rate of R, whereas the urban area has a reduced recharge rate, R_c (Fig. 2b), which is calculated by:

$$R_c = (1 - 2w_B^*)R \quad (4)$$

where $w_B^* = \frac{w_B}{W}$, w_B is half of the length of the urban area perpendicular to the flow direction [L], and W is the aquifer length perpendicular to the flow direction [L] (Fig. 1b). Given that the groundwater flow is purely advective, the groundwater TTD can be expressed by the flux-weighted average of three sub-systems (Leray et al., 2016):

$$\rho_T(a) = \sum_{i=0}^{2} \lambda_\mathrm{i} \rho_\mathrm{i}(a) \quad (5)$$

where λ_i is the weight of the recharge in the *i* th sub-system [-], and $\rho_i(a)$ is the TTD in the *i* th sub-system.

In the following subsections, we derive the explicit expressions of groundwater TTDs in unconfined aquifers intersected by a local urban area (Urban Scenario I) and by a regional urban area (Urban Scenario II), respectively.

2.3.1 Urban Scenario I: aquifer intersected by a local urban area

This subsection provides the explicit expressions of groundwater TTDs for three sub-systems in Urban Scenario I. In the downgradient zone, the aquifer is recharged by the diffuse recharge on the upper boundary. Besides, it is also recharged by the upgradient section of the aquifer. The total inflow for the downgradient zone, Q_{in}, can be expressed as:

$$Q_{in}(\zeta) = R(L - l + w_A - 4w_A w_B^* + \zeta) \tag{6}$$

where ζ is the distance to the downgradient end of the urban area [L] and l is the distance from the center of the urban area to the downgradient boundary [L] (Fig. 2b). The fluid velocity, $v(\zeta)$, is only dependent on the horizontal position ζ, and it can be expressed as:

$$v(\zeta) = \frac{R(L - l + w_A - 4w_A w_B^* + \zeta)}{\theta h(\zeta)} \tag{7}$$

Because the mounding of the water table is small compared to the length of the aquifer, the mean thickness of the downgradient saturated aquifer, $\overline{H}_d$, can be used to approximate $h(\zeta)$: $h(\zeta) \approx \overline{H}_d$, and $\overline{H}_d$ can be calculated using Eq. (37) in Appendix A.

The transit time of water parcel recharged at the position ζ can be determined through integrating the inverse of $v(\zeta)$:

$$\begin{aligned} a(\zeta) &= \int_{\zeta}^{l-w_A} \left[\frac{R(L - l + w_A - 4w_A w_B^* + \zeta)}{\theta \overline{H}_d}\right]^{-1} d\zeta \\ &= \tau_d \ln \frac{L - 4w_A w_B^*}{L - l + w_A - 4w_A w_B^* + \zeta} \end{aligned} \tag{8}$$

where τ_d is expressed as:

$$\tau_d = \frac{\theta \overline{H}_d}{R} \tag{9}$$

Then, the inverse function of $a(\zeta)$, $\zeta(a)$, is expressed as:

$$\zeta(a) = (L - 4w_A w_B^*) \exp\left(-\frac{a}{\tau_d}\right) - (L - l + w_A - 4w_A w_B^*), \qquad a < a_0 \tag{10}$$

where

$$a_0 = \tau_d \ln \frac{L - 4w_A w_B^*}{L - l + w_A - 4w_A w_B^*} \tag{11}$$

Eq. (10) describes the relationship between the recharge position and its corresponding transit time. Hence, the outflux with an age inferior or equal to a, $Q_{out}(a)$, can be expressed as:

$$Q_{out}(a) = R[l - w_A - \zeta(a)] \tag{12}$$

The cumulative TTD for water parcels recharged from the downgradient zone, $P_d(a)$, equals to the mass fraction of outflux with a transit time inferior or equal to a (Etcheverry & Perrochet, 2000):

$$P_d(a) = \frac{Q_{out}(a)}{Q_{out}} \tag{13}$$

where Q_{out} is the total outflux $[L^2T^{-1}]$. The probability density function (pdf) of TTD for downgradient recharge, $\rho_0(a)$, is then expressed as:

$$\rho_0(a) = \frac{dP_d(a)}{da} = \frac{1}{Q_{out}} \frac{dQ_{out}(a)}{da} \tag{14}$$

Combining Eq. (10), Eq. (12), and Eq. (14), the TTD of water parcels recharged from the downgradient zone can be expressed as:

$$\rho_0(a) = \begin{cases} \dfrac{L - 4w_A w_B^*}{\tau_d(l - w_A)} \exp\left(-\dfrac{a}{\tau_d}\right), & a < a_0 \\ 0, & a \geq a_0 \end{cases} \tag{15}$$

The MTT for water mass recharged from the downgradient zone, τ_0, is determined by:

$$\tau_0 = \left(1 + \frac{L - l + w_A - 4w_A w_B^*}{l - w_A} \ln \frac{L - l + w_A - 4w_A w_B^*}{L - 4w_A w_B^*}\right) \tau_d \tag{16}$$

In the urban area, the recharge rate is reduced by the impervious urban area as shown in Eq. (4). The derivation of TTDs for water parcels recharged in this zone is similar to that in the downgradient zone, except for the fact that it experiences a lag to reach the discharge area (Małoszewski & Zuber, 1982). The TTD for water recharged from the urban area, $\rho_1(a)$, is expressed as:

$$\rho_1(a) = \frac{L - l + w_A - 4w_A w_B^*}{2w_A \tau_c (1 - 2w_B^*)} \exp\left(-\frac{a - a_0}{\tau_c}\right), \qquad a_0 \leq a < a_1 \tag{17}$$

where a_0 is determined using Eq. (11), and

$$\tau_c = \frac{\theta_0 \overline{H}_c}{R(1 - 2w_B^*)} \tag{18}$$

$$a_1 = a_0 + \Delta a_1 \tag{19}$$

$$\Delta a_1 = \tau_c \ln \frac{L - l + w_A - 4w_A w_B^*}{L - l - w_A} \tag{20}$$

$\overline{H}_c$ is the mean saturated thickness in the urban area [L], which can be expressed as Eq. (38) in Appendix A.

The MTT for water parcels recharged from the urban area, τ_1, is given by:

$$\tau_1 = \left[1 + \frac{L - l - w_A}{2w_A(1 - 2w_B^*)} \ln \frac{L - l - w_A}{L - l + w_A - 4w_A w_B^*}\right] \tau_c + a_0 \tag{21}$$

The derivation of groundwater TTD for the upgradient zone is similar to that in the urban area, which means it also has an exponential form with a shift a_1:

$$\rho_2(a) = \begin{cases} 0, & a < a_1 \\ \frac{1}{\tau_u}\left(-\frac{a - a_1}{\tau_u}\right), & a \geq a_1 \end{cases} \tag{22}$$

where

$$\tau_u = \frac{\theta \overline{H}_u}{R} \tag{23}$$

The mean saturated thickness for the upgradient zone, $\overline{H}_u$, is expressed by Eq. (39) in Appendix A.

Similarly, the MTT for water parcels recharged from the upgradient zone, τ_2, is expressed as:

$$\tau_2 = \tau_u + a_1 \tag{24}$$

Having derived individual TTDs for three independent sub-systems, we can now assemble them to estimate the overall TTD. The groundwater TTDs for the whole aquifer, $\rho_T(a)$, can be simply expressed as a mass-weighted average of three individual TTDs:

$$\rho_T(a) = \begin{cases} \dfrac{1}{\tau_d}\exp\left(-\dfrac{a}{\tau_d}\right), & a < a_0 \\ \dfrac{L - l + w_A - 4w_A w_B^*}{\tau_c(L - 4w_A w_B^*)}\exp\left(-\dfrac{a - a_0}{\tau_c}\right), & a_0 \leq \ a < a_1 \\ \dfrac{L - l - w_A}{\tau_u(L - 4w_A w_B^*)}\left(-\dfrac{a - a_1}{\tau_u}\right), & a \geq a_1 \end{cases} \tag{25}$$

Eq. (25) can be expressed using a dimensionless form. To that end, we define the following dimensionless parameters:

$$a^* = \frac{a}{\tau_p}, \qquad \tau^* = \frac{\tau}{\tau_p}, \qquad l^* = \frac{l}{L}, \qquad w_A^* = \frac{w_A}{L}, \qquad d^* = \frac{d}{H_L} \tag{26}$$

where *d* is the depth of the urban area below the downstream fixed head [L]. With these dimensionless parameters, Eq. (25) can be transformed into the following dimensionless form:

$$\rho_T(a^*) = \begin{cases} \dfrac{1}{\tau_d}\exp\left(-\dfrac{\tau_p a^*}{\tau_d}\right), & a < a_0^* \\ \dfrac{1 - l^* + w_A^* - 4w_A^* w_B^*}{\tau_c(1 - 4w_A^* \, w_B^*)}\exp\left[-\dfrac{\tau_p(a^* - a_0^*)}{\tau_c}\right], & a_0^* \leq \ a < a_1^* \\ \dfrac{1 - l^* - w_A^*}{\tau_u(1 - 4w_A^* w_B^*)}\exp\left[-\dfrac{\tau_p(a^* - a_1^*)}{\tau_u}\right], & a \geq a_1^* \end{cases} \tag{27}$$

Similarly, the MTT for the whole aquifer can also be expressed by calculating the mass-weighted average of three individual MTTs:

$$\tau^* = \frac{1}{\tau_p}\left(\frac{l^* - w_A^*}{1 - 4w_A^* w_B^*}\tau_0 + \frac{2w_A^* - 4w_A^* w_B^*}{1 - 4w_A^* w_B^*}\tau_1 + \frac{1 - l^* - w_A^*}{1 - 4w_A^* w_B^*}\tau_2\right) \tag{28}$$

where τ_0, τ_1, and τ_2 can be determined using Eq. (16), Eq. (21), and Eq. (24), respectively.

2.3.2 Urban Scenario II: aquifer intersected by a regional urban area

Unlike the above scenario of a local urban area, the scenario of a regional urban area is defined such that it fully penetrates the horizontal boundaries of the aquifer. Hence w_B^* is a constant of 0.5 rather than a variable. Since the bottom of the urban area is beneath the water table, the aquifer section beneath the regional urban area is essentially confined. The derivation of the analytical solution for Urban Scenario II is similar to that for Urban Scenario I, except for the fact that (1) the groundwater recharge in the urban area is completely suppressed by the impervious urban area and (2) no phreatic surface of groundwater exists in the urban area.

Accordingly, the dimensionless form of groundwater TTDs for Urban Scenario II is expressed as:

$$\rho_T(a^*) = \begin{cases} \dfrac{1}{\tau_d}\exp\left(-\dfrac{\tau_p a^*}{\tau_d}\right), & a < a_0^* \\ 0, & a_0^* \leq a < a_1^* \\ \dfrac{1 - l^* - w_A^*}{\tau_u(1 - 2w_A^*)}\exp\left[-\dfrac{\tau_p(a^* - a_1^*)}{\tau_u}\right], & a \geq a_1^* \end{cases} \qquad (29)$$

where τ_p, τ_d, and τ_u can be determined using Eq. (3), Eq. (9), and Eq. (23).

$$a_0^* = \frac{\tau_d}{\tau_p}\ln\frac{1 - 2w_A^*}{1 - l^* - w_A^*} \qquad (30)$$

$$a_1^* = a_0^* + \Delta a_1^*, \qquad \Delta a_1^* = \frac{2w_A^*(1 - d^*)}{1 - l^* - w_A^*} \qquad (31)$$

The MTT for the whole groundwater system, τ^*, is also calculated using the mass-weighted average of two subsystems:

$$\tau^* = \frac{l^* - w_A^*}{1 - 2w_A^*}\tau_0^* + \frac{1 - l^* - w_A^*}{1 - 2w_A^*}\tau_2^* \quad (32)$$

where

$$\tau_0^* = \frac{\tau_d}{\tau_p}\left(1 + \frac{1 - l^* - w_A^*}{l^* - w_A^*}\ln\frac{1 - l^* - w_A^*}{1 - 2w_A^*}\right) \quad (33)$$

$$\tau_2^* = \frac{\tau_u}{\tau_p} + a_1^* \quad (34)$$

2.4 Numerical simulation

We set up numerical models to test the reliability and accuracy of analytical solutions. The numerical codes used in this study are MODFLOW-2005 for the simulation of groundwater flow and MODPATH Version 6 for particle tracking (Harbaugh, 2005; Pollock, 2012). All geometric and hydrogeologic configurations of the numerical model are consistent with the analytical model. Specifically, the test aquifer has a length of 500 m (*L*=500) with a no-flux base and upstream boundary and a fixed head of 10 m ($h_L = 10$) at the downstream boundary. The aquifer is discretized into a 500 × 50 mesh in the horizontal and vertical directions. A large number (2000 ~5000, depending on the scale of the urban area) of particles are released from the phreatic surface of groundwater. The transit time pdfs are estimated using the histogram of transit times of the whole set of particles.

2.5 Sensitivity analysis

To quantify the relative change in TTDs before and after urbanization, we use the normalized form of the mean transit time, τ^*, and the normalized form of variance of transit times, σ^{2*}, as two summary statistics. σ^{2*} is expressed by:

$$\tau^* = \frac{\tau}{\tau_p}, \qquad \sigma^{2*} = \frac{\sigma^2}{\tau_p^2} \tag{35}$$

where σ^2 is the variance of transit times in the urban scenario, and τ_p^2 is the expected variance in the pre-urban scenario where the variance is equal to the square of the mean. These two summary statistics serve as performance metrics for the parametric and sensitivity study.

We applied two approaches to analyze the parametric sensitivity. First, we conducted a local sensitivity analysis focusing on every single parameter; and evaluated their perspective effects on water tables and TTDs. This helps to better understand how the spatial extent and location of the urban area alter the groundwater transit times. Second, we conducted a global sensitivity analysis (GSA) in the full parameter space as well as considering their interactions using Sobolʹ variance-based method. GSA can quantify the interactive contributions among parameters to the total variance in TTDs.

As a variance-based approach, Sobolʹ method has become one of the most popular GSA methods in environmental modeling (Rosolem et al., 2012; Saltelli et al., 1999; Sobol, 2001). Sobolʹ method relates the fraction of the variability in the entity (i.e., the performance metrics) to the variance in the values of various parameters. It typically produces two indices: the first-order sensitivity indices, S_i, and the total-order sensitivity indices, S_{Ti}. The S_i index specifies the individual contribution of factor *i* to the total variance in performance metrics, whereas the S_{Ti} index quantifies the contribution from both individual parameters and the interactions among them to the total variability in performance metrics (Rosolem et al., 2012).

The adjustable ranges of parameters are shown in Table 1. Parameter ranges are set broadly to incorporate potential urban conditions based on the problem conceptualization in Fig.

1 and Fig. 2. Since transit times are independent of d^*, there are five parameters to be evaluated for Urban Scenario I (l^*, w_A^*, w_B^*, R, and K). With w_B^* being fixed, the total number of adjustable parameters for Urban Scenario II is also five (l^*, w_A^*, d^*, R, and K).

Table 1 Adjustable ranges and default values of parameters (See Fig. 2 for more schematic representation).

Parameter	Expression	Description	Lower bound	Upper bound	Default value
l^* (-)	$\frac{l}{L}$	Distance from the center of the urban area to the downstream boundary (normalized)	0.35	0.65	0.50
w_A^* (-)	$\frac{w_A}{L}$	Half of the urban area length in the flow direction (normalized)	0.05	0.25	0.20
w_B^* (-)	$\frac{w_B}{W}$	Half of the urban area length perpendicular to the flow direction (normalized)	0.00	0.50	0.30
d^* (-)	$\frac{d}{h_L}$	Depth of urban structures below the downstream fixed head (normalized)	0.00	0.90	0.50
R (m/yr)	-	Recharge rate	0.10	0.30	0.15
K (m/s)	-	Saturated hydraulic conductivity	1.0×10^{-5}	6.0×10^{-5}	2.0×10^{-5}

3 Results

In this section, we first display the detailed comparison between the TTDs derived from analytical and numerical solutions. We also show the results of the sensitivity analysis, including the sensitivity analysis for individual parameters and the GSA using Sobol′ method.

3.1 Verification of the analytical solution

We first set up six scenarios, ranging from Val1 to Val6, for the verification of analytical solutions. The parameter values for these scenarios are shown in Table 2. Note that Val1 represents the pre-urban scenario, whereas Val2 to Val4 represent Urban Scenario 1, and Val5 to Val6 belong to Urban Scenario 2. As shown in Table 1, the parameter settings in Val5 and Val6 are identical to Val3 and Val 4, respectively, except for the fixed value of w_B^*.

Table 2 Parameter settings for six verification scenarios.

Parameter	Val1	Val2	Val3	Val4	Val5	Val6
l^* (-)	0.00	0.50	0.55	0.40	0.55	0.40
w_A^* (-)	0.00	0.20	0.15	0.10	0.15	0.10
w_B^* (-)	0.00	0.10	0.30	0.40	0.50	0.50
d^* (-)	-	-	-	-	0.70	0.20
R (m/yr)	0.20	0.10	0.15	0.25	0.15	0.25
K (m/s)	2.0×10^{-5}	2.0×10^{-5}	6.0×10^{-5}	2.0×10^{-5}	6.0×10^{-5}	2.0×10^{-5}

The verification results of analytical solutions for six verification scenarios are shown in Fig. 3. As can be seen from Fig. 3, the derived TTDs using analytical solutions correspond well with those using numerical methods for all six verification scenarios. Some minor discrepancies between analytical and numerical results can be found in Val1, wherein the analytical method seems to slightly underestimate the frequency of early breakthrough and overestimate the frequency of the late breakthrough of water parcels. This minor discrepancy could be due to the simplification of using the average value to represent the sloping water table. This discrepancy is less pronounced for urban scenarios since the water table mounding in subsystems is smaller than that in the entire aquifer system, which can be further evidenced by the good correspondence between analytical and numerical results from Fig. 3b to f. For both Urban Scenario I and II, the results from analytical solutions fit well with those estimated from numerical models. The urban areas significantly modify the shapes of TTDs, leading to abrupt changes in TTDs across the urban area (Fig. 3).

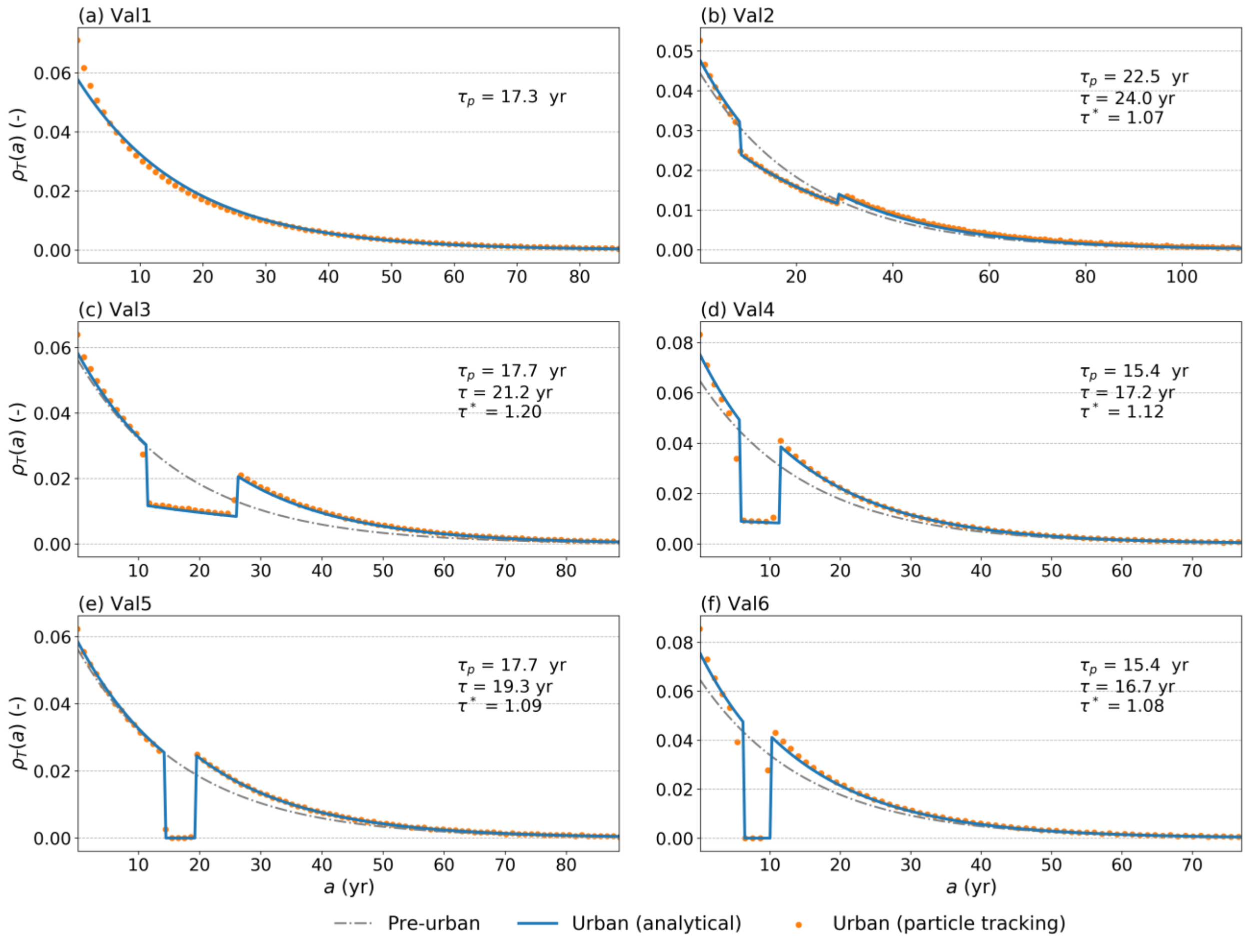

Fig. 3. Verification and comparisons of analytical solutions for groundwater TTDs in six verification scenarios.

The simulated flow pathlines marked by their transit times in six verification scenarios are shown in Fig. 4. From this figure, we can see different organizations of flow pathlines in Urban Scenario I (Val2 to Val4) and Urban Scenario II (Val5 and Val6). Phreatic surfaces can be observed in urban areas in Urban Scenario I, whereas in Urban Scenario II, the corresponding aquifer section is confined by the impervious urban area (Fig. 4). Besides, a small portion of flow pathlines with extremely old ages can be observed at the bottom of the aquifer (denoted by the red color), which corresponds with the long tails of TTDs (Fig. 3). Overall, through the comparisons with the numerical simulations, the analytical solution seems accurate in characterizing groundwater TTDs.

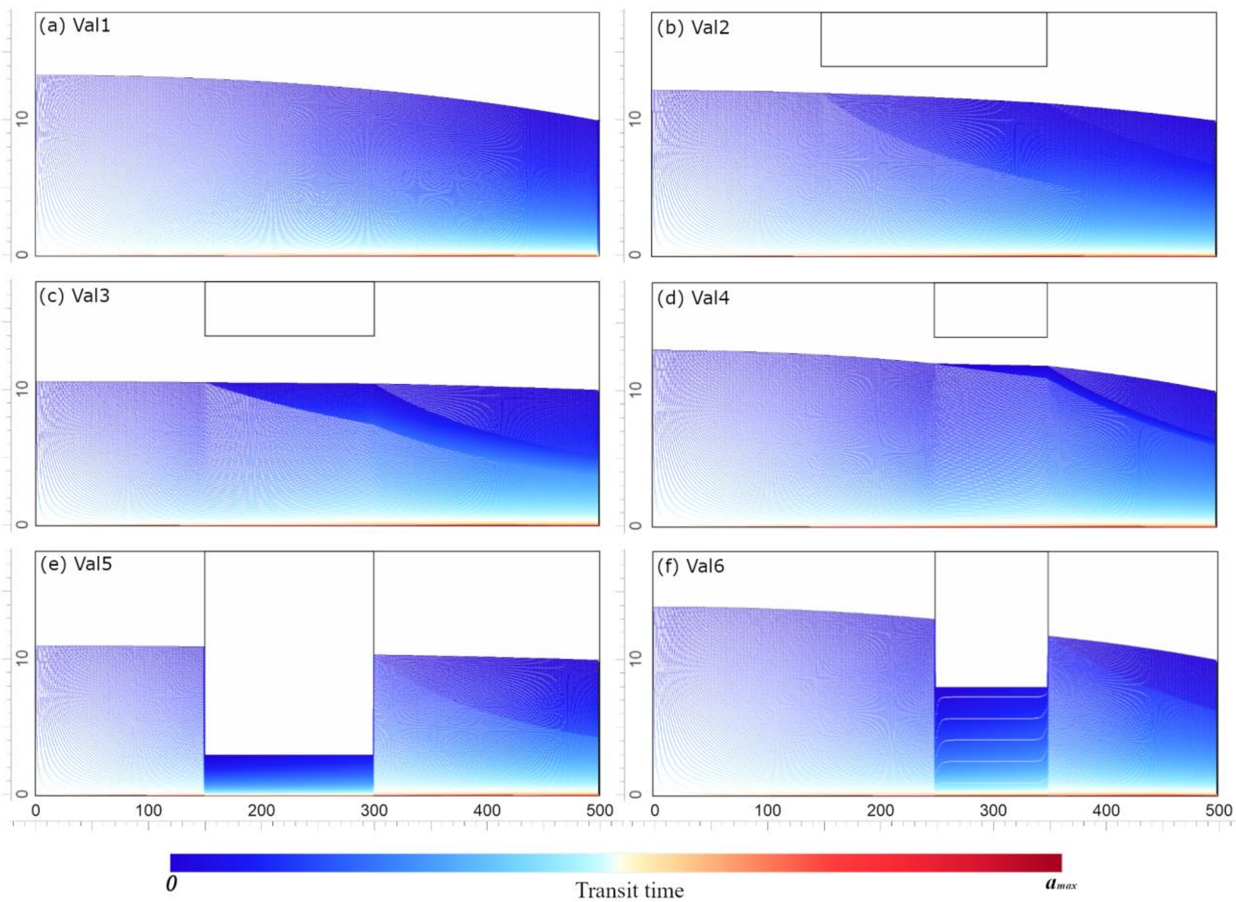

Fig. 4. Simulated flow pathlines marked by the corresponding transit times in six verification scenarios. a_{max} is the maximum transit time in each scenario.

3.2 Influence on the water table

Groundwater TTDs are closely related to the water table, as higher water tables lead to longer transit times as long as the recharge rate does not change (indicated by Eq. (3)). It is, therefore, necessary to evaluate the influence of the impervious urban area on the water table before evaluating the influence on TTDs. Fig. 5 reveals the influence of urbanization on water tables in two urban scenarios. In Urban Scenario I, the impervious urban area tends to drop the water table compared to the pre-urban scenario. Specifically, the drop of the water table in the upgradient zone is greater than that in the downgradient zone. The position of the urban area, l^*, has a marginal impact on the water table, whereas the lengths in the horizontal directions, w_A^* and w_B^*, strongly control the drop in the water table.

These above-mentioned correlations also hold for Urban Scenario II, except for the depth of the urban area, d^* (Fig. 5). In Urban Scenario I, d^* does not impact the water table because the transmissivity in the urban area depends on the height of the phreatic surface. However, in Urban Scenario II, the upgradient water table increases with d^*, which is because the urban structure diminishes the transmissivity by confining the aquifer and reducing the saturated aquifer thickness.

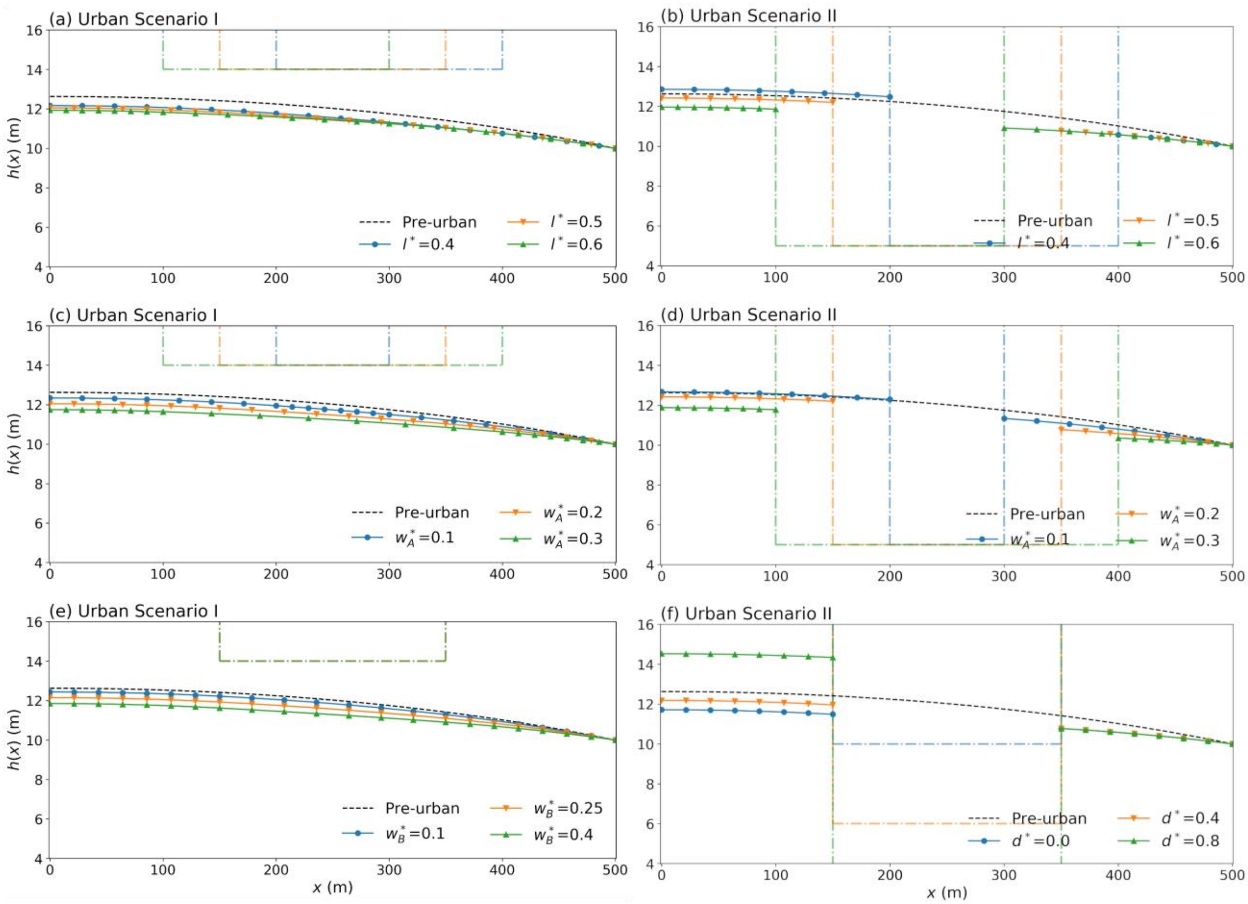

Fig. 5. Responses of the water table to model parameters in two urban scenarios.

Overall, in Urban Scenario I, the urbanization decreases the water table on both the upgradient and the downgradient zones, whereas, in Urban Scenario II, the upgradient water table can be either higher or lower than the pre-urban one, depending on the horizontal extent and depth of the urban area. The distance from the urban area to the downstream boundary appears to have a minor influence on the water table.

3.3 Influence on groundwater TTDs

This subsection presents a sensitivity analysis to investigate the sensitivity of the groundwater TTDs to individual parameters. Here we present results on the sensitivity for two summary statistics to model parameters (see Appendix B for the sensitivity of the entire pdfs of TTDs).

Sensitivities of the normalized MTT, τ^*, to six model parameters in two scenarios are shown in Fig. 6. Those six model parameters can be classified into construction-related parameters (l^*, w_A^*, w_B^*, and d^*) and aquifer-related parameters (*R* and *K*). Our results indicate that l^* has only a minor influence on τ^* in Urban Scenario I, which is consistent with its marginal influence on the water table. In Urban Scenario II, τ^* is more sensitive to l^* than in Urban Scenario I. There is also a positive correlation between τ^* and w_A^* for both two scenarios, which is not surprising since the sealing of urban areas reduces the recharge and slows down the movement of groundwater. What stands out from Fig. 6c is the abrupt drop when the urban area transits from local to regional, i.e., when the urban structure interferes with the natural groundwater flow. This is because the confinement of the aquifer section reduces the water transit times across the urban area due to the reduction in aquifer transmissivity. τ^* has a non-monotonous correlation with d^* in Urban Scenario II (Fig. 6c). This is because the regional urban area impacts τ^* in two ways. First, external disturbance of the aquifer section through the introduction of urban areas reduces the total pore space and increases the fluid velocity. Accordingly, transit times across the urban area are reduced. Second, the urban structure reduces the aquifer transmissivity and lifts the water table in the upgradient zone, therefore increases the transit times of water recharged upgradient. Depending on the interplay between these two cases, τ^* experiences an early drop followed by a rise with d^*, and the minimum τ^* occurs when d^* equals 0.71 (Fig. 6d).

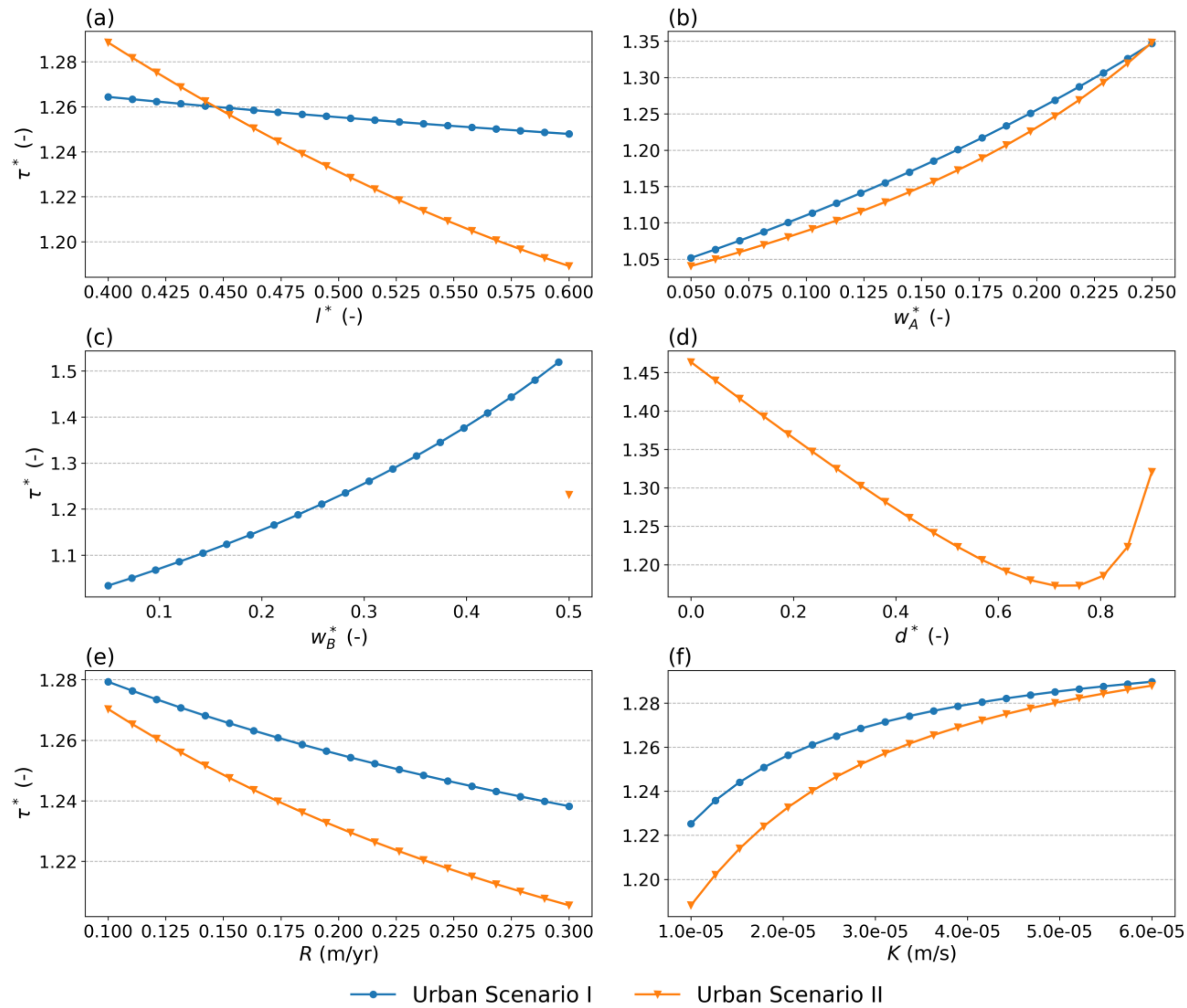

Fig. 6. Sensitivities of τ^* to model parameters in two urban scenarios.

Except for those construction-related parameters, TTDs are not independent of the aquifer-related parameters (R and K). Specifically, τ^* and σ^{2*} correlate negatively with R, whereas they correlate positively with K. This can be attributed to the different degrees of changes in water tables with varying R and K as indicated in Fig. 5g and i.

In addition to τ^*, we also investigated the sensitivities of the normalized variance of transit times, σ^{2*}, to model parameters in two scenarios (Fig. 7). As shown in Fig. 7, σ^{2*} is positively correlated with l^* and w_A^* in both scenarios. σ^{2*} also increases with w_B^* in Urban Scenario I (Fig. 7c). Similar to the correlation between τ^* and d^*, σ^{2*} has a non-monotonous correlation with d^*, which is also attributed to the interplay between the increase in transit times across the upgradient zone and the decrease in transit times across the urban area. Two aquifer-related parameters, *R* and *K*, however, appear to have minor effects on the total variance in σ^{2*} as indicated by the small fluctuations in τ^* (Fig. 7e and f).

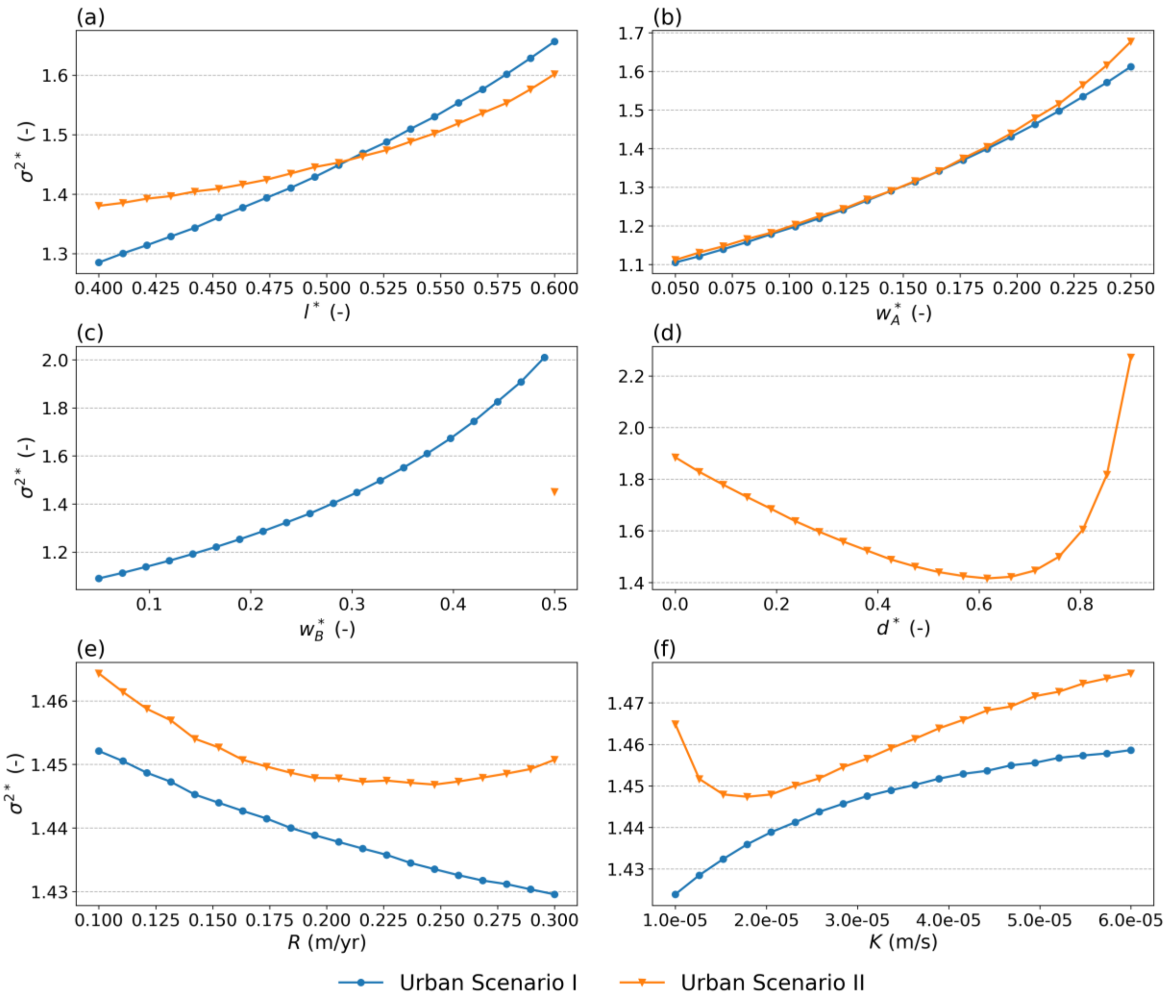

Fig. 7. Sensitivities of σ^{2*} to model parameters in two urban scenarios.

3.4 Sobol′ sensitivity indices for model parameters

The above local sensitivity analysis reveals the relationship between summary statistics and individual parameters. The GSA in this subsection focuses more on disentangling the influences of individual parameters and interactions among them on the summary statistics. Fig**.** 8 displays Sobol′ sensitivity indices for τ^* and σ^{2*} in two urban scenarios. In Urban Scenario I, the variance in τ^* is strongly controlled by the horizontal lengths of the urban area, and it is not sensitive to R and K. In contrast, σ^{2*} is not only sensitive to horizontal lengths but also the position of the urban area. In Urban Scenario II, τ^* is most sensitive to w_A^* and d^* with S_{Ti} of 0.67 and 0.38, and σ^{2*} is dominantly controlled by w_A^*, l^*, and d^*. The contributions from aquifer-related parameters, i.e., R and K, to the variances in τ^* and σ^{2*} are quite limited compared to those construction-related parameters. In both scenarios, the variances in τ^* are mainly controlled by the direct influence of parameters. By contrast, the indirect influence (i.e., the interaction among parameters) significantly contributes to the variance in σ^{2*}. This indicates that the urban area has a potentially greater disturbance on the variance of transit times than the MTT.

Overall, Sobol′ sensitivity analysis reveals that the parameter sensitivity depends on the chosen summary metrics. Despite the urban scenario, τ^* and σ^{2*} appear to be most sensitive to the horizontal size of the urban area. They are also strongly controlled by d^* in urban scenario II.

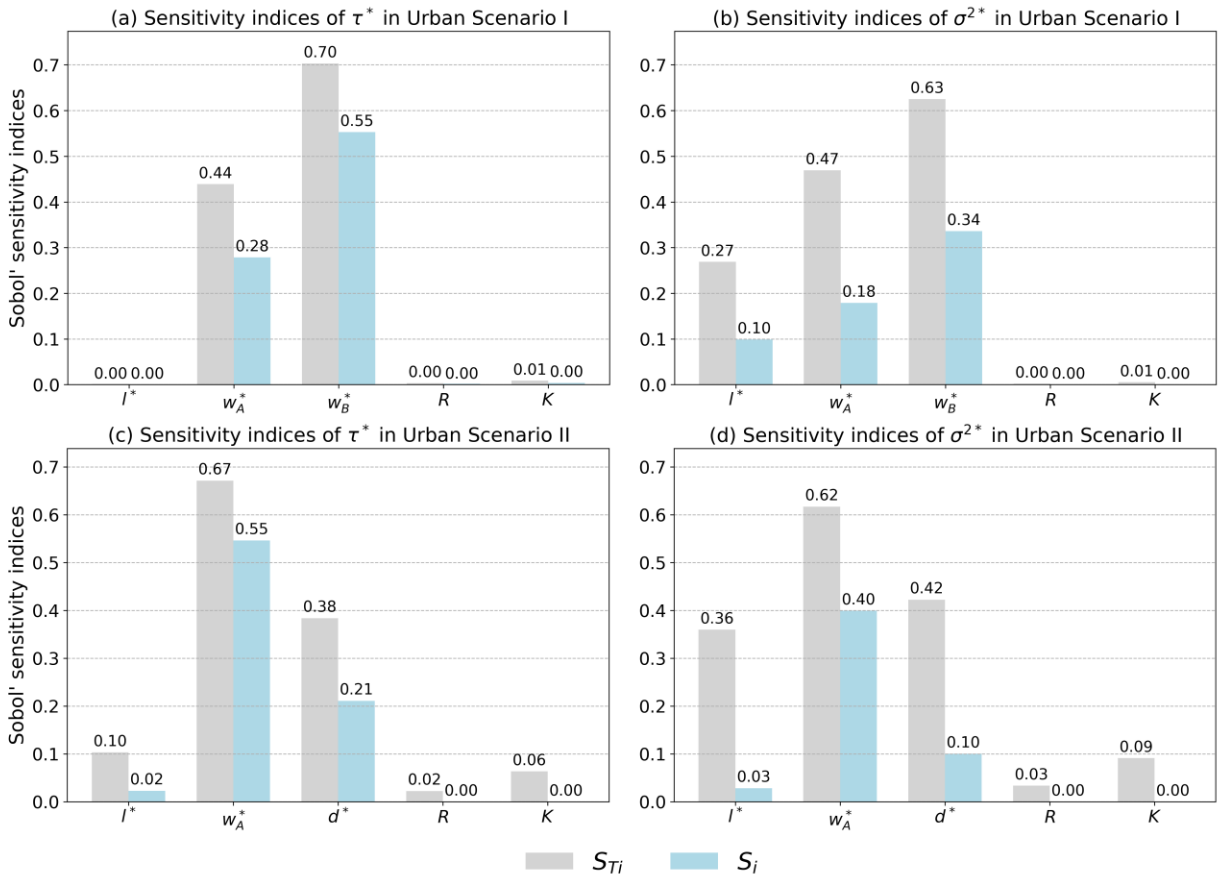

Fig. 8. Sobol′ sensitivity analysis for two summary statistics in two urban scenarios. S_{Ti} denotes total-order sensitivity indices, and S_i denotes first-order sensitivity indices.

4 Discussion

4.1 Implications for urban water resources management

Pujades et al. (2012) have defined the barrier effect of underground construction as the "*increase in head loss across the construction area relative to the natural head loss before construction*". They found that the underground structure tends to increase the head difference when intersecting the confined aquifers. However, Pujades et al. (2012) have assumed that the total flux through the aquifer remains unchanged after the construction. Font-Capo et al. (2015)

further developed a method to identify the barrier effect based on the response time of piezometers in pumping tests. Our study suggests that the head loss across the urban area can be either higher or smaller than that in the pre-urban case depending on the spatial extent and depth of the urban area (Fig. 5). This does not contradict the findings from Pujades et al. (2012) because their solutions are built on the assumptions of a confined aquifer and an unchanged total recharge. By contrast, our study aims to reveal the regional behavior of groundwater transit times affected by a large-scale urban area, wherein the modification of recharge by the impervious area cannot be neglected (Lerner, 2002; Voisin et al., 2018).

In a rapidly urbanizing world, many agricultural catchments are influenced by the expansion of urban areas. Urbanization introduces additional organic contaminants into the regional groundwater system that threatens the surface water and groundwater quality (Jurado et al., 2012; Larsen et al., 2016). Through the derived analytical solutions, our study further reveals the potentially prolonged MTT in both urban settings compared to pre-urban conditions. This prolonged MTT is mainly due to the prevention of recharge by the impervious zones in Urban Scenario II. In contrast, it may also be induced from the rise in the upgradient water table as indicated by Eq. (23). Meanwhile, the increase in MTT may be partially compensated by the decrease in aquifer transmissivity beneath the constructed zone. The increase in groundwater transit times may cause the lag in the response of stream water to the nonpoint-source contamination (e.g., nitrogen and phosphorus). This lag could amplify the response time of the stream water to nonpoint-source contamination, which could further endanger the goal of maintaining good surface water quality (Chen et al., 2014; Jing et al., 2021; Van Meter et al., 2017).

The increased σ^{2*} in the urban aquifer system indicates the potential divergence in the transit times of water parcels recharged upgradient and downgradient. This implies the fates of nonpoint-source contaminants are also influenced by the impervious urban zone (Parajulee et al., 2019; Soulsby et al., 2015). While the contaminants recharged from the downgradient zone mainly flow in the shallow part of the aquifer and have short transit times, those recharged upgradient may have deep flow paths and tailing behaviors.

4.2 Implications for urban planning

A major goal of urban water resources management is to restore the flow regime and freshwater quality to the natural condition, which has been widely accepted as a hydrological objective for urban water resources management (Bonneau et al., 2017; Fatahi Nafchi et al., 2021; Jefferson et al., 2017; Poff et al., 1997). As a key component of the water cycle, the restoration of groundwater quantity and quality is critical for achieving this goal. This study shows that urbanization shifts the groundwater system onto a new trajectory by altering the water table and transit times, which may not be recovered to the pre-development condition. With the biased mean and variance of transit times from the natural ones, it is only possible to minimize the urban disturbance to groundwater transit times. This finding is in line with the results of Jefferson et al. 2017, wherein they suggested that the restoration of pre-urban hydrology and water quality is rarely achieved in practice.

Our in-depth analysis of the parametric uncertainty with different sensitivity approaches has great implications for the planning of large-scale urban construction projects. It shows that (1) the expansion of urban areas will inevitably exacerbate the deviation of groundwater TTDs, and (2) the interplay between urban area and aquifer must be considered when assessing the environmental risk of urban construction. When the urban area is large enough to fully penetrate the horizontal boundaries and deep enough to intersect with the water table, there exists an optimal depth of construction whereby the disturbance of construction to the MTT is minimal (Fig. 6d). This depth of the urban construction has great implications for urban planning as it suggests the reference depth of construction that disturbs the groundwater transit times the least. The sensitivity analysis further highlights that the spatial relationship between the urban area and the aquifer should be primarily accounted for when planning the urban construction project. Accordingly, the suggested analytical model benefits urban planning by providing decision-making support for the environmental risk assessment.

4.3 Advantages and limitations of the analytical model

The proposed analytical model has all distinguishing attributes of close-formed equations. An obvious advantage lies in the fact that all parameters of our analytical model can be derived from hydrogeological and geographic information. That being said, TTDs can be directly approximated employing the proposed analytical model without the use of environmental tracers. Another advantage of the analytical solution lies in its robustness in the characterization of the discontinuous TTDs, which is often the case in urban groundwater systems. Deriving TTDs by direct sampling of particles suffer from numerical errors (Yang et al., 2021). If the number of particles or the discretization of the time step is insufficient, the probability distributions derived from numerical tracking may deviate from reality. In this regard, the analytical approach is more promising in characterizing the discontinuous TTDs. Besides, the high computational efficiency of the proposed analytical model permits the easy implementation of the computationally expensive GSA.

As a simplified model relying on certain prior assumptions, the analytical model inevitably has some limitations. The analytical solution is only valid for the homogeneous nature of a porous medium and does not apply to highly heterogeneous media wherein the preferential flow in fractures may dominate the groundwater circulation pattern. The analytical model also implicitly assumes that the free surface of the unconfined aquifer can be represented by the water table. However, Cheng et al. (2021) found that the water table equation is not self-consistent. Nevertheless, the discrepancy between the free surface and water table is small relative to the total saturated thickness and therefore has a marginal influence on the regional groundwater TTDs. Another limitation is that the groundwater mounding has to be small to moderate, otherwise the derived groundwater TTDs would significantly deviate from the reality (Abrams & Haitjema, 2018; Haitjema, 1995). This implies that the groundwater head difference between the upgradient and downgradient boundaries should be primarily evaluated before applying the proposed analytical model. Besides, the analytical model does not account for any leakages from water mains or sewage pipes, which may underestimate the total recharge and overestimate the MTT.

5 Conclusions

We have developed an analytical model for groundwater TTDs in urban unconfined aquifers intersected by an impervious urban area. The solution has been derived for a purely advective flow system in a homogeneous aquifer under steady-state conditions. Following the Dupuit-Forchheimer assumption and assuming a small to moderate groundwater mounding, we have derived the explicit expressions for the water tables, the pdfs of TTDs, and the MTTs.

The analytical solution seems correct through the comparisons with numerical solutions using particle tracking. A comprehensive analysis of parametric uncertainty shows that the local impervious urban area lowers down the water table, while the regional impervious urban area can either increase or decrease the upgradient water table. The urban area tends to increase the groundwater MTT despite the urban scenario. Groundwater TTDs show varying degrees of sensitivities to model parameters in two urban scenarios. While the groundwater MTT is only sensitive to the horizontal size of the urban area in Urban Scenario I, it is sensitive to both the horizontal size and the vertical extension of the urban area in Urban Scenario II. Furthermore, there appears to be an optimal depth of the impervious urban structure that minimizes the disturbance of urbanization to the groundwater transit times in Urban Scenario II. Accordingly, the spatial relationship between the urban area and the aquifer should be considered in priority when inferring the groundwater TTDs.

As a first-order approximation of the complex real-world groundwater system, the developed analytical model complements the existing analytical transit time models and provides additional information on influences from imperviousness and interference with natural groundwater flow. Being computationally efficient and easy to implement, it provides decision-making support for regional water resources management and urban planning.

Appendix A: Solutions for the mean saturated thickness

In the pre-urban scenario, the mean saturated thickness of the whole domain, $\overline{H}$, can be calculated by integrating Eq. (1):

$$\overline{H} = \frac{h_L}{2} + \sqrt{\frac{R}{K}}\left(\frac{L}{2} + \frac{Kh_L^2}{2RL}\right)\arcsin\frac{L}{\sqrt{L^2 + \frac{Kh_L^2}{R}}} \tag{36}$$

The derivation of mean saturated thickness in the urban scenario is similar to that in the pre-urban scenario. In this scenario, the mean thickness of the downgradient saturated aquifer, $\overline{H}_d$, can be expressed by:

$$\begin{aligned}\overline{H}_d = \frac{\sqrt{\frac{R}{K}}}{l - w_A}\Bigg\{&\frac{L - 4w_A w_B^*}{2}\sqrt{\psi^2 - (L - 4w_A w_B^*)^2} + \frac{\psi^2}{2}\arcsin\frac{L - 4w_A w_B^*}{\psi}\\ &- \frac{L - l + w_A - 4w_A w_B^*}{2}\sqrt{\psi^2 - [L - l + w_A(1 - 4w_B^*)]^2}\\ &- \frac{\psi^2}{2}\arcsin\frac{L - l + w_A - 4w_A w_B^*}{\psi}\Bigg\}\end{aligned} \tag{37}$$

where $\psi = \sqrt{(L - 4w_A w_B^*)^2 + \frac{K}{R}h_L^2}$.

The mean saturated thickness in the urban area, $\overline{H}_c$, can be expressed as:

$$\begin{aligned}\overline{H}_c = \frac{\sqrt{\frac{R}{K}}}{2w_A(1 - 2w_B^*)}\Bigg[&\frac{L - l + w_A - 4w_A w_B^*}{2}\sqrt{\psi - (L - l + w_A - 4w_A w_B^*)^2}\\ &+ \frac{\psi^2}{2}\arcsin\frac{L - l + w_A - 4w_A w_B^*}{\psi}\\ &- \frac{L - l - w_A}{2}\sqrt{\psi^2 - (L - l - w_A)^2} - \frac{\psi^2}{2}\arcsin\frac{L - l - w_A}{\psi}\Bigg]\end{aligned} \tag{38}$$

where $\psi = \sqrt{(L - 4w_A w_B^*)^2 + \frac{K}{R} h_L^2}$.

The mean saturated thickness for the upgradient zone, $\overline{H}_u$, is expressed as:

$$\overline{H}_u = \frac{h_u}{2} + \sqrt{\frac{R}{K}} \left[\frac{L - l - w_A}{2} + \frac{K h_u^2}{2R(L - l - w_A)} \right] \arcsin \frac{L - l - w_A}{\sqrt{(L - l - w_A)^2 + \frac{K h_u^2}{R}}} \quad (39)$$

where h_u is the water table at the downgradient end of the upgradient zone [L], which is given by:

$$h_u = \sqrt{\frac{4Rw_A}{K} (L - l - 2w_A w_B^*) + h_d^2} \quad (40)$$

Appendix B: Full transit time pdfs in two urban scenarios

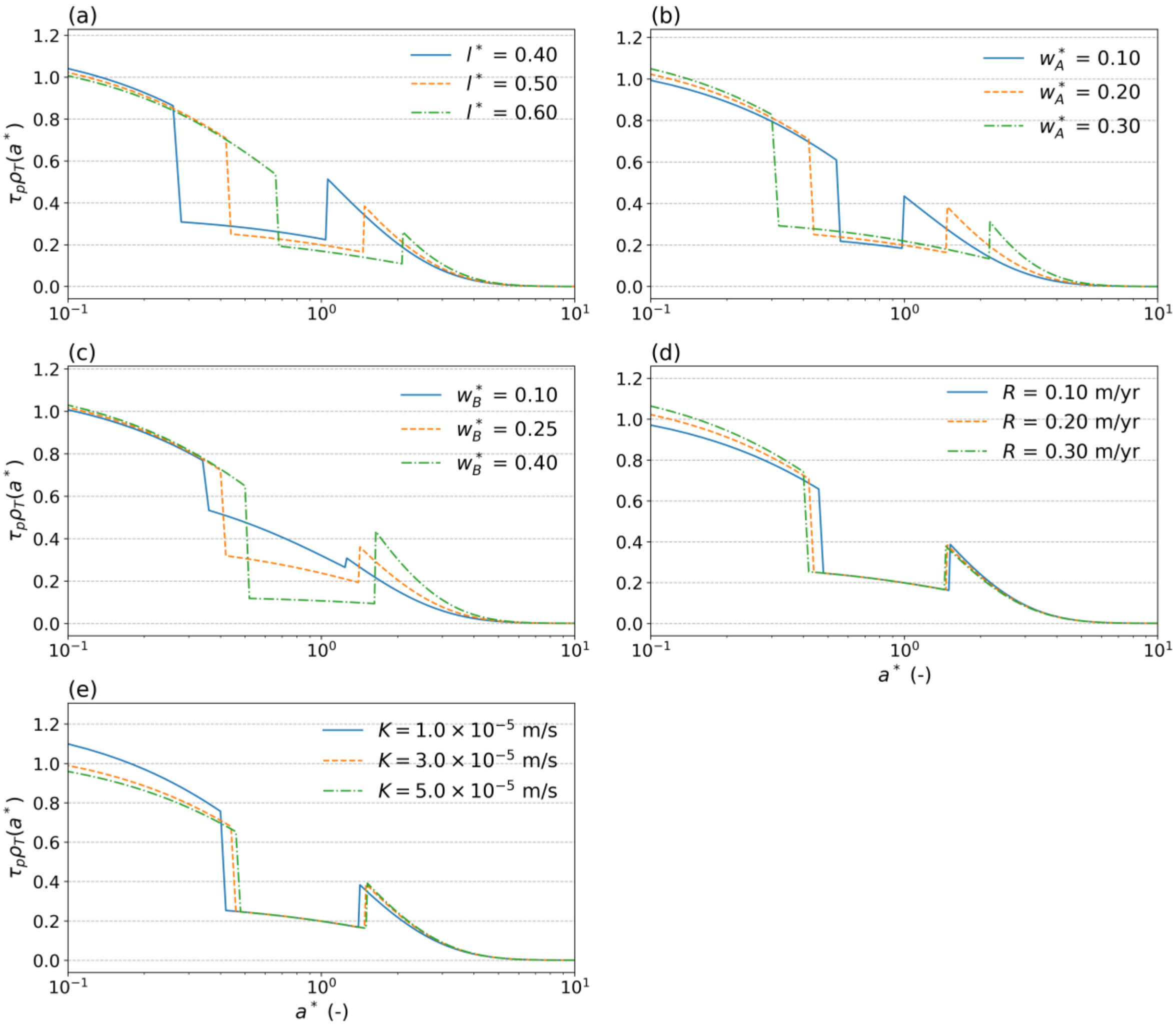

Figure A1. Transit time pdfs using sampled parameter values in Urban Scenario I.

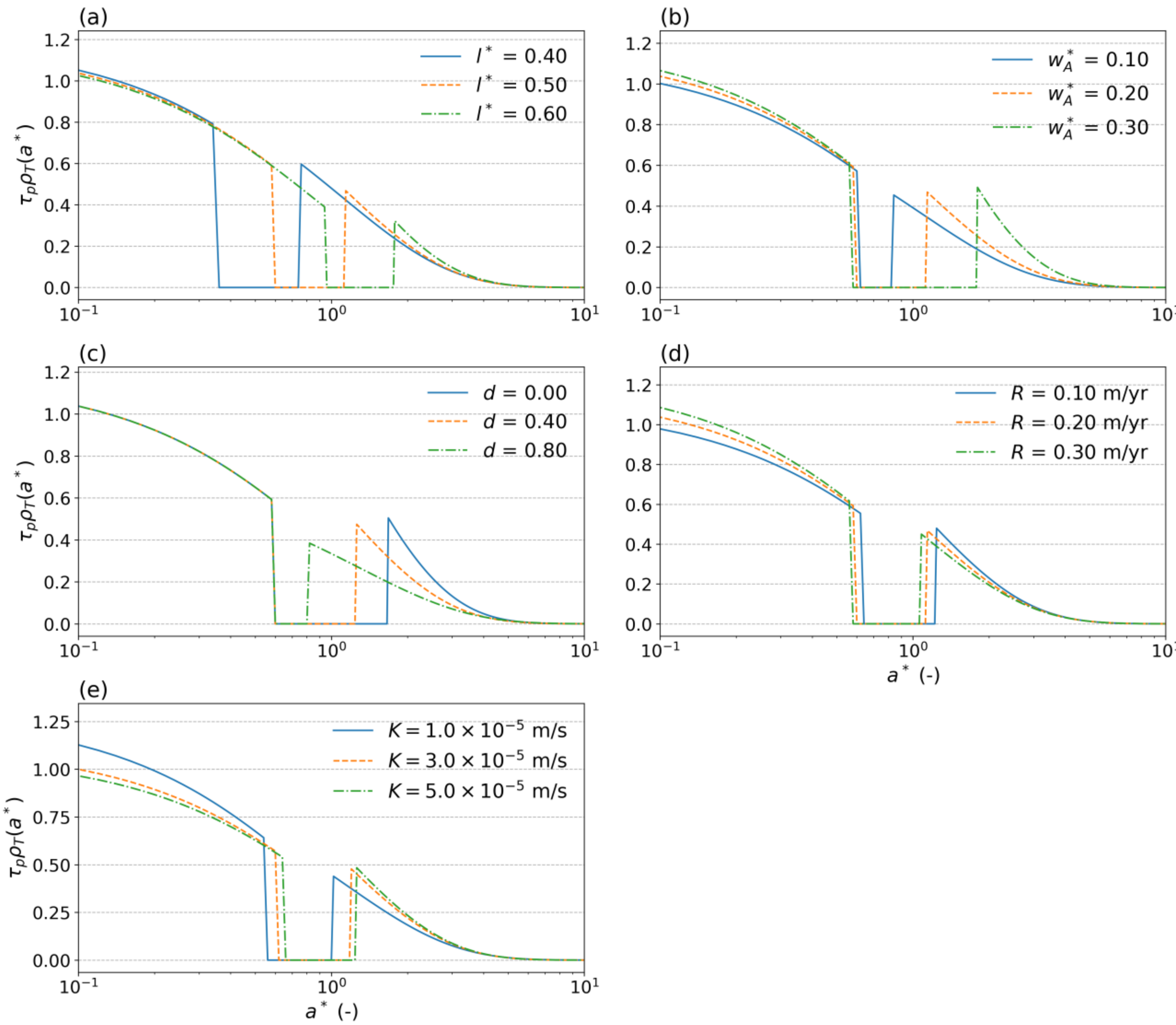

Figure A2. Transit time pdfs using sampled parameter values in Urban Scenario II.

Acknowledgments

C. Lu acknowledges the financial support from the National Natural Science Foundation of China (51679067 and 51879088), Fundamental Research Funds for the Central Universities (B200204002), and the Natural Science Foundation of Jiangsu Province (BK20190023).

References

Abrams, D., & Haitjema, H. (2018). How Aquifer Characteristics of a Watershed Affect Transit Time Distributions of Groundwater. *Groundwater*, *56*(4), 517–520. https://doi.org/10.1111/gwat.12788

Asadollahi, M., Stumpp, C., Rinaldo, A., & Benettin, P. (2020). Transport and Water Age Dynamics in Soils: A Comparative Study of Spatially Integrated and Spatially Explicit Models. *Water Resources Research*, *56*(3), 1–17. https://doi.org/10.1029/2019wr025539

Attard, G., Rossier, Y., & Eisenlohr, L. (2016). Urban groundwater age modeling under unconfined condition - Impact of underground structures on groundwater age: Evidence of a piston effect. *Journal of Hydrology*, *535*, 652–661. https://doi.org/10.1016/j.jhydrol.2016.02.034

Attard, G., Rossier, Y., & Eisenlohr, L. (2017). Underground structures increasing the intrinsic vulnerability of urban groundwater: Sensitivity analysis and development of an empirical law based on a groundwater age modelling approach. *Journal of Hydrology*, *552*, 460–473. https://doi.org/10.1016/j.jhydrol.2017.07.013

Attard, G., Winiarski, T., Rossier, Y., & Eisenlohr, L. (2016). Review: Impact of underground structures on the flow of urban groundwater. *Hydrogeology Journal*, *24*(1), 5–19. https://doi.org/10.1007/s10040-015-1317-3

Basu, N. B., Jindal, P., Schilling, K. E., Wolter, C. F., & Takle, E. S. (2012). Evaluation of analytical and numerical approaches for the estimation of groundwater travel time distribution. *Journal of Hydrology*, *475*, 65–73. https://doi.org/10.1016/j.jhydrol.2012.08.052

Benettin, P., Kirchner, J. W., Rinaldo, A., & Botter, G. (2015). Modeling chloride transport using travel time distributions at Plynlimon, Wales. *Water Resources Research*, *51*(5), 3259–3276. https://doi.org/10.1002/2014WR016600

Benettin, P., Soulsby, C., Birkel, C., Tetzlaff, D., Botter, G., & Rinaldo, A. (2017). Using SAS functions and high-resolution isotope data to unravel travel time distributions in headwater catchments. *Water Resources Research*, *53*(3), 1864–1878. https://doi.org/10.1002/2016WR020117

Bhaskar, A. S., Beesley, L., Burns, M. J., Fletcher, T. D., Hamel, P., Oldham, C. E., & Roy, A. H. (2016). Will it rise or will it fall? Managing the complex effects of urbanization on base flow. *Freshwater Science*, *35*(1), 293–310. https://doi.org/10.1086/685084

Bonneau, J., Burns, M. J., Fletcher, T. D., Witt, R., Drysdale, R. N., & Costelloe, J. F. (2018). The impact of urbanization on subsurface flow paths – A paired-catchment isotopic study. *Journal of Hydrology*, *561*, 413–426. https://doi.org/10.1016/j.jhydrol.2018.04.022

Bonneau, J., Fletcher, T. D., Costelloe, J. F., & Burns, M. J. (2017). Stormwater infiltration and the ‘urban karst’ – A review. *Journal of Hydrology*, *552*, 141–150. https://doi.org/10.1016/j.jhydrol.2017.06.043

Chen, D., Hu, M., & Dahlgren, R. A. (2014). A dynamic watershed model for determining the effects of transient storage on nitrogen export to rivers. *Water Resources Research*, *50*(10), 7714–7730. https://doi.org/https://doi.org/10.1002/2014WR015852

Cheng, D., Zhan, H., Li, J., & Cheng, D. (2021). Characteristics of inverted saturated zone under unclogged streams. *Journal of Hydrology*, *597*, 126288. https://doi.org/https://doi.org/10.1016/j.jhydrol.2021.126288

Connor, R. (2015). *The United Nations world water development report 2015: Water for a sustainable world* (Vol. 1). UNESCO publishing.

Danesh-Yazdi, M., Klaus, J., Condon, L. E., & Maxwell, R. M. (2018). Bridging the gap between numerical solutions of travel time distributions and analytical storage selection functions. *Hydrological Processes*, *32*(8), 1063–1076. https://doi.org/10.1002/hyp.11481

Dupuit, J. É. J. (1863). *Études théoriques et pratiques sur le mouvement des eaux dans les canaux découverts et à travers les terrains perméables: avec des considérations relatives au régime des grandes eaux, au débouché à leur donner, et à la marche des alluvions dans les rivièr*. Dunod.

Eberts, S. M., Böhlke, J. K., Kauffman, L. J., & Jurgens, B. C. (2012). Comparison of particle-tracking and lumped-parameter age-distribution models for evaluating vulnerability of production wells to contamination. *Hydrogeology Journal*, *20*(2), 263–282. https://doi.org/10.1007/s10040-011-0810-6

Engdahl, N. B., & Maxwell, R. M. (2015). Quantifying changes in age distributions and the hydrologic balance of a high-mountain watershed from climate induced variations in recharge. *Journal of Hydrology*, *522*, 152–162. https://doi.org/10.1016/j.jhydrol.2014.12.032

Eriksson, E. (1958). The Possible Use of Tritium' for Estimating Groundwater Storage. *Tellus*, *10*(4), 472–478. https://doi.org/https://doi.org/10.1111/j.2153-3490.1958.tb02035.x

Etcheverry, D., & Perrochet, P. (2000). Direct simulation of groundwater transit-time distributions using the reservoir theory. *Hydrogeology Journal*, *8*(2), 200–208.

Fatahi Nafchi, R., Yaghoobi, P., Reaisi Vanani, H., Ostad-Ali-Askari, K., Nouri, J., & Maghsoudlou, B. (2021). Eco-hydrologic stability zonation of dams and power plants using the combined models of SMCE and CEQUALW2. *Applied Water Science*, *11*(7), 109. https://doi.org/10.1007/s13201-021-01427-z

Font-Capo, J., Pujades, E., Vàzquez-Suñé, E., Carrera, J., Velasco, V., & Montfort, D. (2015). Assessment of the barrier effect caused by underground constructions on porous aquifers with low hydraulic gradient: A case study of the metro construction in Barcelona, Spain. *Engineering Geology*, *196*, 238–250. https://doi.org/https://doi.org/10.1016/j.enggeo.2015.07.006

Forchheimer, P. (1886). Über die Ergiebigkeit von Brunnen-Anlagen und Sickerschlitzen. In *des Arch-and-Ing-Verein zu Hannover* (pp. 539–563).

Ginn, T. R., Haeri, H., Massoudieh, A., & Foglia, L. (2009). Notes on groundwater age in forward and inverse modeling. *Transport in Porous Media*, *79*(1 SPEC. ISS.), 117–134. https://doi.org/10.1007/s11242-009-9406-1

Golian, M., Katibeh, H., Singh, V. P., Ostad-Ali-Askari, K., & Rostami, H. T. (2020). Prediction of tunnelling impact on flow rates of adjacent extraction water wells. *Quarterly Journal of Engineering Geology and Hydrogeology*, *53*(2), 236–251. https://doi.org/10.1144/qjegh2019-055

Haitjema, H. M. (1995). On the residence time distribution in idealized groundwater sheds. *Journal of Hydrology*, *172*, 127–146.

Hamel, P., & Fletcher, T. D. (2014). Modelling the impact of stormwater source control infiltration techniques on catchment baseflow. *Hydrological Processes*, *28*(24), 5817–5831. https://doi.org/10.1002/hyp.10069

Harbaugh, A. W. (2005). MODFLOW-2005 , The U . S . Geological Survey Modular Ground-Water Model — the Ground-Water Flow Process. *U.S. Geological Survey Techniques and Methods*.

Havril, T., Tóth, Á., Molson, J. W., Galsa, A., & Mádl-Szonyi, J. (2018). Impacts of predicted climate change on groundwater flow systems: Can wetlands disappear due to recharge reduction? *Journal of Hydrology*, *563*, 1169–1180. https://doi.org/10.1016/j.jhydrol.2017.09.020

Heße, F., Zink, M., Kumar, R., Samaniego, L., & Attinger, S. (2017). Spatially distributed characterization of soil-moisture dynamics using travel-time distributions. *Hydrology and Earth System Sciences*, *21*(1), 549–570. https://doi.org/10.5194/hess-21-549-2017

Hrachowitz, M., & Clark, M. P. (2017). HESS Opinions: The complementary merits of competing modelling philosophies in hydrology. *Hydrology and Earth System Sciences*, *21*(8), 3953–3973. https://doi.org/10.5194/hess-21-3953-2017

Janke, B. D., Finlay, J. C., Hobbie, S. E., Baker, L. A., Sterner, R. W., Nidzgorski, D., & Wilson, B. N. (2014). Contrasting influences of stormflow and baseflow pathways on nitrogen and phosphorus export from an urban watershed. *Biogeochemistry*, *121*(1), 209–228. https://doi.org/10.1007/s10533-013-9926-1

Jefferson, A. J., Bhaskar, A. S., Hopkins, K. G., Fanelli, R., Avellaneda, P. M., & McMillan, S. K. (2017). Stormwater management network effectiveness and implications for urban watershed function: A critical review. *Hydrological Processes*, *31*(23), 4056–4080. https://doi.org/10.1002/hyp.11347

Jing, M., Heße, F., Kumar, R., Kolditz, O., Kalbacher, T., & Attinger, S. (2019). Influence of input and parameter uncertainty on the prediction of catchment-scale groundwater travel time distributions. *Hydrology and Earth System Sciences*, *23*(1), 171–190. https://doi.org/10.5194/hess-23-171-2019

Jing, M., Kumar, R., Attinger, S., Li, Q., Lu, C., & Heße, F. (2021). Assessing the contribution of groundwater to catchment travel time distributions through integrating conceptual flux tracking with explicit Lagrangian particle tracking. *Advances in Water Resources*, *149*, 103849. https://doi.org/10.1016/j.advwatres.2021.103849

Jing, M., Kumar, R., Heße, F., Thober, S., Rakovec, O., Samaniego, L., & Attinger, S. (2020). Assessing the response of groundwater quantity and travel time distribution to 1.5, 2, and 3 °C global warming in a mesoscale central German basin. *Hydrology and Earth System Sciences*, *24*(3), 1511–1526. https://doi.org/10.5194/hess-24-1511-2020

Jurado, A., Vàzquez-Suñé, E., Carrera, J., López de Alda, M., Pujades, E., & Barceló, D. (2012). Emerging organic contaminants in groundwater in Spain: A review of sources, recent occurrence and fate in a European context. *Science of the Total Environment*, *440*, 82–94. https://doi.org/10.1016/j.scitotenv.2012.08.029

Kuhlemann, L. M., Tetzlaff, D., & Soulsby, C. (2020). Urban water systems under climate stress: An isotopic perspective from Berlin, Germany. *Hydrological Processes*, *34*(18), 3758–3776. https://doi.org/10.1002/hyp.13850

Kumar, R., Heße, F., Rao, P. S. C., Musolff, A., Jawitz, J. W., Fleckenstein, J. H., Rakovec, O., Thober, S., & Attinger, S. (2020). Strong hydroclimatic controls on vulnerability to subsurface nitrate contamination across Europe. *Nature Communications*, 1–10. https://doi.org/10.1038/s41467-020-19955-8

Kuppel, S., Tetzlaff, D., Maneta, M. P., & Soulsby, C. (2020). Critical Zone Storage Controls on the Water Ages of Ecohydrological Outputs. *Geophysical Research Letters*, *47*(16), e2020GL088897. https://doi.org/10.1029/2020GL088897

Larsen, T. A., Hoffmann, S., Lüthi, C., Truffer, B., & Maurer, M. (2016). Emerging solutions to the water challenges of an urbanizing world. *Science*, *352*(6288), 928–933. https://doi.org/10.1126/science.aad8641

Leray, S., Engdahl, N. B., Massoudieh, A., Bresciani, E., & McCallum, J. (2016). Residence time distributions for hydrologic systems: Mechanistic foundations and steady-state analytical solutions. *Journal of Hydrology*, *543*, 67–87. https://doi.org/10.1016/j.jhydrol.2016.01.068

Lerner, D. N. (2002). Identifying and quantifying urban recharge: A review. *Hydrogeology Journal*, *10*(1), 143–152. https://doi.org/10.1007/s10040-001-0177-1

Luo, J., & Cirpka, O. A. (2008). Traveltime-based descriptions of transport and mixing in heterogeneous domains. *Water Resources Research*, *44*(9). https://doi.org/https://doi.org/10.1029/2007WR006035

Małloszewski, P., & Zuber, A. (1992). On the calibration and validation of mathematical models for the interpretation of tracer experiments in groundwater. *Advances in Water Resources*, *15*(1), 47–62. https://doi.org/10.1016/0309-1708(92)90031-V

Małoszewski, P., & Zuber, A. (1982). Determining the turnover time of groundwater systems with the aid of environmental tracers: 1. Models and their applicability. *Journal of Hydrology*, *57*(3–4), 207–231.

McCallum, J. L., Cook, P. G., & Simmons, C. T. (2015). Limitations of the Use of Environmental Tracers to Infer Groundwater Age. *Groundwater*, *53*(S1), 56–70. https://doi.org/10.1111/gwat.12237

McCance, W., Jones, O. A. H., Edwards, M., Surapaneni, A., Chadalavada, S., & Currell, M. (2018). Contaminants of Emerging Concern as novel groundwater tracers for delineating wastewater impacts in urban and peri-urban areas. *Water Research*, *146*, 118–133. https://doi.org/10.1016/j.watres.2018.09.013

Ostad-Ali-Askar, K., Su, R., & Liu, L. (2018). Water resources and climate change. *Journal of Water and Climate Change*, *9*(2), 239. https://doi.org/10.2166/wcc.2018.999

Ostad-Ali-Askari, K., Ghorbanizadeh Kharazi, H., Shayannejad, M., & Zareian, M. J. (2019). Effect of management strategies on reducing negative impacts of climate change on water resources of the Isfahan–Borkhar aquifer using MODFLOW. *River Research and Applications*, *35*(6), 611–631. https://doi.org/https://doi.org/10.1002/rra.3463

Ostad-Ali-Askari, K., Kharazi, H. G., Shayannejad, M., & Mohammad, J. Z. (2020). Effect of Climate Change on Precipitation Patterns in an Arid Region Using GCM Models: Case Study of Isfahan-Borkhar Plain. *Natural Hazards Review*, *21*(2), 4020006. https://doi.org/10.1061/(ASCE)NH.1527-6996.0000367

Ostad-Ali-Askari, K., & Shayannejad, M. (2021). Quantity and quality modelling of groundwater to manage water resources in Isfahan-Borkhar Aquifer. *Environment,* *Development and Sustainability*, *23*(11), 15943–15959. https://doi.org/10.1007/s10668-021-01323-1

Parajulee, A., Wania, F., & Mitchell, C. P. J. (2019). Hydrological transit times in nested urban and agricultural watersheds in the Greater Toronto Area, Canada. *Hydrological Processes*, *33*(3), 350–360. https://doi.org/10.1002/hyp.13328

Poff, N. L. R., Allan, J. D., Bain, M. B., Karr, J. R., Prestegaard, K. L., Richter, B. D., Sparks, R. E., & Stromberg, J. C. (1997). The natural flow regime: A paradigm for river conservation and restoration. *BioScience*, *47*(11), 769–784. https://doi.org/10.2307/1313099

Pollock, D. W. (2012). User Guide for MODPATH Version 6—A Particle-Tracking Model for MODFLOW. *Section A, Groundwater Book 6, Modeling Techniques*, 58 p.

Pujades, E., Jurado, A., Carrera, J., Vázquez-Suñé, E., & Dassargues, A. (2016). Hydrogeological assessment of non-linear underground enclosures. *Engineering Geology*, *207*, 91–102. https://doi.org/10.1016/j.enggeo.2016.04.012

Pujades, E., López, A., Carrera, J., Vázquez-Suñé, E., & Jurado, A. (2012). Barrier effect of underground structures on aquifers. *Engineering Geology*, *144–145*, 41–49. https://doi.org/10.1016/j.enggeo.2012.07.004

Raats, P. A. C. (1977). Convective transport of solutes by steady flows II. Specific flow problems. *Agricultural Water Management*, *1*(3), 219–232. https://doi.org/https://doi.org/10.1016/0378-3774(77)90002-6

Remondi, F., Botter, M., Burlando, P., & Fatichi, S. (2019). Variability of transit time distributions with climate and topography: A modelling approach. *Journal of Hydrology*, *569*, 37–50. https://doi.org/10.1016/j.jhydrol.2018.11.011

Rosolem, R., Gupta, H. V., Shuttleworth, W. J., Zeng, X., & De Gonçalves, L. G. G. (2012). A fully multiple-criteria implementation of the Sobol' method for parameter sensitivity analysis. *Journal of Geophysical Research: Atmospheres*, *117*(7), 1–18. https://doi.org/10.1029/2011JD016355

Saltelli, A., Tarantola, S., & Chan, K. P. S. (1999). A quantitative model-independent method for global sensitivity analysis of model output. *Technometrics*, *41*(1), 39–56. https://doi.org/10.1080/00401706.1999.10485594

Schwartz, S. S., & Smith, B. (2014). Slowflow fingerprints of urban hydrology. *Journal of Hydrology*, *515*, 116–128. https://doi.org/10.1016/j.jhydrol.2014.04.019

Sobol, I. M. (2001). Global sensitivity indices for nonlinear mathematical models and their Monte Carlo estimates. *Mathematics and Computers in Simulation*, *55*(1–3), 271–280. https://doi.org/10.1016/S0378-4754(00)00270-6

Soulsby, C., Birkel, C., Geris, J., & Tetzlaff, D. (2015). Spatial aggregation of time-variant stream water ages in urbanizing catchments. *Hydrological Processes*, *29*(13), 3038–3050. https://doi.org/10.1002/hyp.10500

Stewart, M. K., Morgenstern, U., & McDonnell, J. J. (2010). Truncation of stream residence time: how the use of stable isotopes has skewed our concept of streamwater age and origin. *Hydrological Processes*, *24*(12), 1646–1659.

Talebmorad, H., Abedi-Koupai, J., Eslamian, S., Mousavi, S.-F., Akhavan, S., Ostad-Ali-Askari, K., & Singh, V. P. (2021). Evaluation of the impact of climate change on reference crop evapotranspiration in Hamedan-Bahar plain. *International Journal of Hydrology Science and Technology*, *11*(3), 333–347. https://doi.org/10.1504/IJHST.2021.114554

Van Der Velde, Y., De Rooij, G. H., Rozemeijer, J. C., Van Geer, F. C., & Broers, H. P. (2010). Nitrate response of a lowland catchment: On the relation between stream concentration and travel time distribution dynamics. *Water Resources Research*, *46*(11), 1–17. https://doi.org/10.1029/2010WR009105

Van Meter, K. J., Basu, N. B., & Van Cappellen, P. (2017). Two centuries of nitrogen dynamics: Legacy sources and sinks in the Mississippi and Susquehanna River Basins. *Global Biogeochemical Cycles*, *31*(1), 2–23. https://doi.org/10.1002/2016GB005498

Vázquez-Suñé, E., Carrera, J., Tubau, I., Sánchez-Vila, X., & Soler, A. (2010). An approach to identify urban groundwater recharge. *Hydrology and Earth System Sciences*, *14*(10), 2085–2097. https://doi.org/10.5194/hess-14-2085-2010

Vázquez-Suñé, E., Sánchez-Vila, X., & Carrera, J. (2005). Introductory review of specific factors influencing urban groundwater, an emerging branch of hydrogeology, with reference to Barcelona, Spain. *Hydrogeology Journal*, *13*(3), 522–533. https://doi.org/10.1007/s10040-004-0360-2

Voisin, J., Cournoyer, B., Vienney, A., & Mermillod-Blondin, F. (2018). Aquifer recharge with stormwater runoff in urban areas: Influence of vadose zone thickness on nutrient and bacterial transfers from the surface of infiltration basins to groundwater. *Science of the Total Environment*, *637–638*, 1496–1507. https://doi.org/10.1016/j.scitotenv.2018.05.094

Xu, Y. S., Yan, X. X., Shen, S. L., & Zhou, A. N. (2019). Experimental investigation on the blocking of groundwater seepage from a waterproof curtain during pumped dewatering in an excavation. *Hydrogeology Journal*, *27*(7), 2659–2672. https://doi.org/10.1007/s10040-019-01992-3

Yang, C., Zhang, Y.-K., Liang, X., Olschanowsky, C., Yang, X., & Maxwell, R. (2021). Accelerating the Lagrangian particle tracking of residence time distributions and source water mixing towards large scales. *Computers & Geosciences*, *151*, 104760. https://doi.org/https://doi.org/10.1016/j.cageo.2021.104760

Zuber, A. (1986). On the interpretation of tracer data in variable flow systems. *Journal of Hydrology*, *86*(1), 45–57. https://doi.org/10.1016/0022-1694(86)90005-3